LA-UR-74-937 (Revised)

Conf-740645--2

TITLE: High Rate Physical Vapor Deposition of Refractory Metals

AUTHOR(S): Max A. Sherman, Rointan F. Bunshan, and Harry A. Beale

SUBMITTED TO: 1974 Vacuum Metallurgy Conference

Pittsburgh, Pennsylvania

June 17 - 20, 1974

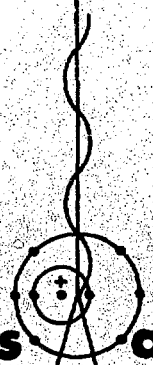

los alamos
scientific laboratory
of the University of California
LOS ALAMOS, NEW MEXICO 87544

Form No. 836
St. No. 2629
1/73

UNITED STATES
ATOMIC ENERGY COMMISSION
CONTRACT W-7405-ENG. 36

High Rate Physical Vapor Deposition of Refractory Metals *

Max A. Sherman
Los Alamos Scientific Laboratory
Los Alamos, New Mexico 87544

and

Rointan F. Bunshah
Materials Department, University of California
Los Alamos, California 90024

and

Harry A. Beale
Pratt and Whitney Aircraft
East Hartford, Connecticut 06108

Mechanical properties of Mo, Nb and V bulk deposits produced by high rate physical vapor deposition techniques (HRPVD) were studied. Deposits were characterized by impurity content, grain size and morphology, yield strength, hardness and bend ductility. The lattice parameter, tensile strength and tensile ductility were also determined for Mo. They were vapor deposited at $0.37T_m$, with Mo further studied from $0.23\text{-}0.44T_m$ (where T_m is the absolute melting temperature).

Yield strengths of Mo and Nb were comparable to those of wrought material having equivalent grain sizes. An average yield strength of $36.1\ kg/mm^2$ (51.5 ksi) was obtained in V deposits of 0.7 μm grain size,

* Work performed partially under the auspices of the United States Atomic Energy Commission.

+ Work performed in partial satisfaction of the requirements of the degree of Master of Science, UCLA.

which is well above previously reported values. This high yield strength is primarily due to grain size refinement and not the interstitial content.

Ultra fine grained refractory metals, such as the V deposits produced in this study, may greatly reduce void formation and growth in irradiated materials in fast breeder and controlled thermonuclear reactors. As void growth causes dimensional changes and degradation of mechanical properties in reactor structural components, it is desirable to reduce the problem by removing excess vacancies (produced by the neutron irradiation) which drive the void nucleation and growth process. A calculation shows that this may be accomplished by trapping the vacancies at grain boundaries. For the V of this study, at a typical operating temperature of a controlled thermonuclear reactor first wall (973K), up to 92% of the excess vacancies are trapped at the boundaries for a dislocation density of 10^8 cm^{-2}. This would reduce the dimensional change by an order of magnitude for a given neutron fluence. We suggest that HRPVD techniques may be used to prepare fine-grained materials having superior resistance to swelling induced by fast neutron irradiation.

INTRODUCTION

Metals irradiated by fast neutrons between 0.3 and 0.5 of their absolute melting temperatures T_m swell by a void formation and growth process as a function of fluence, temperature, gas content, and microstructure. This is a major obstacle to development of fast breeder and controlled thermonuclear reactors, due to dimensional changes and degradation of mechanical properties of structural components. In addition, hydrogen embrittlement and transmutation (conversion of one isotope to another) are expected to cause problems. For example, niobium, one of the current reference structural materials for the first wall of a theta-pinch controlled thermonuclear reactor (CTR) design (Fig. 1),[1] is expected to suffer swelling rates of 1-5%/year, a transmutation rate (to Zr, Mo, Y) of 1.4 at.%/year, and 890 at.ppm/year H production (Table I) at an annual fluence of 2.84×10^{21} neutrons/cm^2. To successfully operate such a reactor will require development of first wall materials that resist swelling, to minimize their periodic and costly replacement.

The objective of this study was to investigate the microstructure and yield strength relationships of three possible CTR first wall candidate materials - Mo, Nb and V - produced by high rate physical vapor deposition (HRPVD) techniques at various deposition temperatures. We wanted to determine if one could use HRPVD techniques, where microstructure of deposits can be controlled, to prepare materials having superior resistance to swelling than wrought material.

EXPERIMENTAL TECHNIQUES

A schematic of the vapor deposition setup is shown in Fig. 2. The evaporant stock, a 2.5 cm diameter billet, is mounted in a rod fed electron-beam-heated evaporation source. The evaporant was condensed on direct or indirect resistance heated substrates. The substrates were thin rolled foils of the same material as the evaporant. The entire assembly was mounted in a stainless steel vacuum bell jar. The pressure during depositon was 1×10^{-5} to 1×10^{-4} torr. Two chromel-alumel thermocouples were spot welded to the back side of the substrates to monitor condensation temperature.

To synthesize these deposits, the substrates were heated to the desired deposition temperature prior to heating the evaporant billet. The electron beam was turned on to form the molten pool at the end of the billet as the vapor source, with a shutter positioned over the pool to protect the substrate from initial spitting. Upon removing the shutter to begin the deposition, the heater current was lowered to compensate for the radiant heat transfer to the substrate from the pool. During deposition on direct resistance heated substrates, the current was gradually increased to offset the effect of increasing cross-sectional area of the condensate. After the initial temperature transient, substrate temperatures could be controlled to $\pm$ 5K. Deposition rates ranged from 0.5 μm/min. to 12.7 μm/min. and deposit thicknesses from 25 μm to 325 μm.

Tensile specimens were cut from the center of the deposits, and machined to size with a rotary-blade carbide burr. The tensile specimen gage length was 2.5 cm, the gage width typically about 0.6 cm, and the thickness

was ∿ 0.3 mm. Thickness variations in the gage length were usually 4-6%.

Vickers microhardness measurements were taken on polished metallographic specimens, with ten indentations made on both a surface and edge of each sample to permit a statistical treatment. Bend tests were performed according to ASTM specification E290-68[2].

The lattice parameters of Mo deposits were measured for samples deposited between 673K and 1263K. The reflections from the (200) through the (400) peaks were used, isolating the $K_{\alpha 1}$ and $K_{\alpha 2}$ reflections according to the Rachinger technique.[3] The Nelson-Riley extrapolation function was used to obtain the lattice parameter,[4] employing a least squares fit in each case.

RESULTS AND DISCUSSION

Chemical Analysis

Impurity concentrations in the evaporants and deposits are reported in Tables II-IV. The vacuum fusion techique was used to analyze for O_2, N_2, and H_2, the combustion method for C, and mass spectrographic techniques for the metallic impurities.

The impurity content of the deposits result from the condensation of impurities in the gas phase. The metallic impurities come primarily from the melt. The interstitial impurities, O_2,H_2,N_2,and C, are present in the gas phase from the vacuum environment (vacuum gas phase, outgassing from container surface, etc.) as well as due to specific reactions occurring in the melt such as sacraficial deoxidation.[6,7]

Molybdenum. Sample MO-A-5 was synthesized from a Thermo Electron billet and Mo-E-3-3 from Climax stock. The major difference between the Mo deposit

and evaporant composition is the oxygen content (Table II). The increased oxygen content of the deposits is consistent with the prediction[5,6] that a Mo melt will deoxide by Mo suboxide volatitilization, thus transferring oxygen to the deposit and resulting in a higher content relative to the evaporant. The higher impurity contents in the Mo-A-5 deposit made from Thermo Electron stock as compared to Mo-E-3-3 made from Climax Molybdenum stock suggests that the vendor analysis supplied with the former is incorrect.

Niobium. The chemical analysis of niobium evaporant and deposits (Table III) show a marked pickup in O and Ta in the deposits. This also agrees with the prediction [5,6] of sacraficial deoxidation of the melt by TaO and NbO volatilization, thus concentrating oxygen and tantalum in the deposit as shown in the analysis.

Vanadium. The oxygen contamination of vanadium deposits during deposition is due to sacraficial deoxidation of MoO, as evidenced by the molybdenum and oxygen concentration in the deposits. Molybdenum has a much lower vapor pressure than vanadium and therefore the Mo concentration in the deposit cannot be due to evaporation of Mo atoms from the melt.

Grain Size and Morphology

The morphology of deposits is strongly influenced by condensation temperature. Movchan and Demchishin [7] investigated the temperature dependence of morphologies of Ni, Ti, W, Al_2O_3, and ZrO_2 deposits. Bunshah and co-workers[8] found this model to apply for Ti, Ni, Ni-20Cr, and TiC.

They found three morphology zones dependent on homologous temperature (Fig. 3), with transition temperatures T_1 and T_2 between the zones of $T_1 = 0.3T_m$ and $T_2 = 0.3\text{-}0.45T_m$ for metals. Zone 1 ($T<0.3T_m$) has a domed-surface structure with tapered grains, the dome diameter increasing with temperature. Zone 2 ($0.3T_m < T < 0.45\text{-}0.5T_m$) exhibits a columnar grain morphology with a smooth matte surface. In zone 3 ($T>0.45\text{-}0.5T_m$) an equiaxed structure in both surface and cross section was reported. Such transition temperatures calculated from their model for metals of interest here are given in Table V.

Molybdenum. The range of deposition temperatures investigated was 673 to 1263 K. Figure 4 shows the characteristic domed morphology as predicted by the Movchan-Demchishin model. At higher temperatures, the columnar morphology characteristic of zone 2 is to be expected and was confirmed in the investigation for deposition temperatures of 1188-1263 K (0.41-0.44 T_m) with the grain size increasing with temperature. However, in the range 973-1188 K (0.32-0.44 T_m) epitaxial growth occurred on the rolled Mo sheet substrate, and the grain morphology was identical to the elongated grain structure typical of rolled sheet with no increase in grain diameter with temperature. Figure 5 shows a surface view of a Mo deposit with the elongated grain morphology. Figure 6 is a cross-sectional view and shows grain growth of the substrate grains into the deposit. We did not observe such epitaxial growth in V or Nb deposits in the same homologous temperature range. Nor have examples of epitaxial growth of thick deposits been reported.

Niobium. When deposited at $0.37T_m$ (1023K), niobium exhibited an equiaxed structure in both surface and cross section (i.e., a zone 3 morphology) rather than the predicted columnar morphology (Fig. 7). The grain size of the deposits averaged ~9.4 μm.

Vanadium. The vanadium was deposited at 540K ($0.37T_m$). Transmission electron microscopy revealed a grain size of 0.7 μm in the plane of the foil (Fig. 8). A number of small pinholes were introduced during the thinning process, showing up as white dots.

Mechanical Properties

Molybdenum. The yield and ultimate tensile strengths are presented as a function of inverse square root of grain diameter in Figs. 9 and 10. Foils were tested at crosshead speeds of 0.05 and 0.005 cm/min to investigate the effect of strain rate on tensile properties. Hall [9] and Petch [10] proposed the following relation between grain size and yield or flow stress of polycrystalline metals:

$$\sigma = \sigma_o + kd^{-1/2} \qquad (1)$$

where σ = yield or flow stress,
σ_o = function stress,
k = Hall-Petch slope,
d = grain diameter.

Mo obeys this relationship for yield and fracture at both crosshead speeds. The constants σ_o and k, obtained from a least squares fit, are listed in Table VI with other mechanical property data on Mo deposits.

The problem of separating the effects of strain rate and impurity content on yield and tensile strengths is introduced by the substantial differences in purities of deposits tested at the different crosshead speeds. Foils synthesized from Thermo Electron evaporant stock were tested at 0.05 cm/min, and those from the purer Climax Mo at 0.0005 cm/min. Briggs and Campbell [11] found the lower yield stress of Mo to vary linearly with the log of strain rate at room temperature, with a slope of 7.5 kg/mm^2 log sec^{-1}. If we assume that this holds for vapor deposited material, and further assume that a decade change in crosshead speed corresponds to a decade change in strain rate, then σ_o should be 7.5 kg/mm^2 greater at 0.05 cm/min than at 0.005 cm/min. The actual change was 12.3 kg/mm^2. We expect the difference to be due to the increased interstitial content and

the fact that the normalized crosshead speed (speed/gage length) is somewhat larger than the true strain rate. The results of this work are consistent with those previously reported, [12-15] as larger strain rates were used in those investigations, thus increasing σ_o.

Upper and lower yield strengths previously reported for Mo [12-15] were not observed in the study. This may be due to a pre-strain effect introduced while flattening samples in a fixture at 473-573K to hold them in place while machining tensile specimens, thus obliterating the yield points.

Niobium. The yield strengths of niobium deposits are presented in a Hall-Petch plot (Fig. 11), with results on wrought material included for comparison. A wide range of Hall-Petch parameters σ_o and k_y have been obtained [16-22] due to varying strain rates and impurity contents of the test specimens. Szkopiak [22] reviewed the effect of oxygen and nitrogen, the most prevalent interstitials, on σ_o and k_y. He concluded that the increase in yield strength for coarse-grained specimens was 2×10^{-2} per wt. ppm oxygen and 4.14×10^{-4} kg/mm^2 per wt. ppm nitrogen, thereby increasing σ_o and lowering k_y. Briggs and Campbell [11] found the lower yield stress to vary non-linearly with log strain rate, gradually increasing with strain rate. As the strain rate used in this study was lower than in previous investigations, the relatively low yield strengths are consistent with these results. The absence of upper and lower yield points is thought to be due to the same prestrain effect described for molybdenum.

Vanadium. Figure 12 presents the yield strength of vanadium deposits, with findings of previous studies [19,23] for comparison. The large value of σ_o reported by Lindley and Smallman [19] appears to be due to the high oxygen

content (1700 ppm) of their samples. Elssner and Horz [24] determined that the lower yield of the recrystallized material obeyed the relation:

$$\sigma_{LY}(kg/mm^2) = 5.0 + 2.0C_N + 50.0C_O \qquad (2)$$

where 5.0 is the value of σ_{LY} for zero gas content, and C_N and C_O are the nitrogen and oxygen concentrations in atom percent.

For a deposit containing 84 wt. ppm nitrogen and 470 wt. ppm oxygen, the increase in yield from the last two terms of Eq. (2) is 7.6 kg/mm^2. Extrapolation of the data of D. H. Sherman et. al. [23] to $d^{-1/2} = 38\ mm^{-1/2}$ (this work) and adding the impurity correction from Eq. (2) results in a calculated yield of 35.6 kg/mm^2. This is only 0.5 kg/mm^2 below the measured yield, well within experimental error.

None of the samples was loaded to fracture. However, one was strained to 14% elongation. This is somewhat more ductile than the 12% strain reported by Van Fossen [25] for $d^{-1/2} = 7.3\ mm^{-1/2}$ at a strain rate of 0.005/min. It compares favorably with Lindley and Smallman's range [26] of 6% to 22% for $d^{-1/2} = 1.97$ to 11.6 $mm^{-1/2}$.

Hardness

Molybdenum. Belomytsov et. al. [27] measured the microhardness of Mo condensates and reported a dependence on substrate temperature. The hardness was approximately 240 kg/mm^2 (VHN) above a 1023K deposition temperature, increasing to 400 kg/mm^2 at 873K. The measurements in this study for deposition temperatures of 973-1173K averaged 242 kg/mm^2, in excellent agreement with the previous work.

Niobium. The surface and edge hardness values were 115.5 and 119.5 kg/mm^2, respectively. These agree very well with those of Paxton and Sheehan [28]

who reported a Vickers hardness of 120 kg/mm^2 for a 350 wt. ppm oxygen content.

Vanadium. Anisotropy in hardness was observed. The average microhardness is 115.3 kg/mm^2 on the surface and 107.7 kg/mm^2 on the edge.

Bend Ductility

Molybdenum. The bend ductility of the deposits was low, with percent elongation under 1%. The percent elongation is:

$$E = 100T/(D + T) \quad (3)$$

where T = thickness of deposit + substrate

D = mandrel diameter.

The low ductility is attributed to the carbon and oxygen content. Barr et. al.[29] found a large increase in the ductile-brittle transition temperature between 40 and 80 wt. ppm carbon. Maringer and Schwope[30] reported severe grain boundary embrittlement of the oxygen-saturated material. As the oxygen content is above the solubility limit,[31] the low ductility is consistent with these reports. Deposits with much lower oxygen contents can be prepared by prior high vacuum melting of the evaporant stock. This would improve the ductility of the deposits.

Niobium and vanadium. The niobium deposits withstood and average 9.3% elongation (5.4T bend test) before cracking. Vanadium withstood an 18.8% average longation (2.2T bend radius).

Molybdenum Lattice Parameter

The lattice parameter of the molybdenum sheets were found to be independent of substrate temperature, as shown in Figure 13. The impurity contents of the deposits are low enough (Table II) so that contamination

is not considered to be a significant factor, as the deposit purities (99.8857-99.9639%) equal or better those of bulk molybdenum samples for which lattice parameters have been reported by Pearson [32]. The small variation in the lattice parameters is attributed to slight deviations from flatness. The standard deviation from the bulk material lattice parameter at 293K (3.1468Å) [32] is 7.05×10^{-4} Å.

Belomytsov et. al. [27] have previously measured the lattice parameter of molybdenum deposits condensed over a similar temperature range (723-1373K versus 673-1263K in this work). They found a significant decrease below a deposition temperature of 1123K, the difference increasing with decreasing temperature (Fig. 13). However, deposit thicknesses and impurity contents were not reported or considered. Their work may apply only to thin films.

EFFECT OF GRAIN SIZE REFINEMENT ON VOID GROWTH IN IRRADIATED METALS

Metals, when irradiated from 0.3 to $0.5T_m$, swell by a void formation and growth process as a function of fluence, microstructure, purity, and temperature. A fast neurton, slowing done by elastic scattering, creates a damage zone known as a displacement spike containing equal numbers of vacancies and displaced atoms in interstitial sites. These point defects either recombine or migrate to sinks such as dislocations, grain boundaries, and voids. Grain boundaries and dislocations are better sinks for interstitials than vacancies, so that an excess of vacancies results which drives the void nucleation and growth process. By refining the grain size, as with the HRPVD produced vanadium of this study, one increases the total

grain boundary area and hence the effectiveness of grain boundaries as vacancy sinks relative to dislocations and voids. If one can bias vacancy migration to sinks other than voids, one reduces the void growth rate.

Harkness et. al.[33] have developed sink terms describing the flux of point defects to voids, dislocations, grain boundaries, and precipitates. The relative efficiency of a sink is simply:

$$f_{v,j} = Q_{v,j} / \sum_k Q_{v,k} \tag{4}$$

where $f_{v,j}$ is the efficiency of sink j, and

$Q_{v,k}$ is the flux of vacancies to sink k.

Applying (4) to these flux terms,[33] one obtains:

$$f_{v,gb} = [1 + \pi L R_g R_s / 3 \ln(R_s/R_c) + \tfrac{2}{3} \pi R_v X_v R_g R_s]^{-1} \tag{5}$$

$$f_{v,dis} = [1 + 3 \ln(R_s/R_c)/\pi L R_g R_s + \tfrac{L}{2} R_v X_v \ln(R_s/R_c)]^{-1} \tag{6}$$

$$f_{v,void} = [1 + 3/2\pi R_g R_s R_v X_v + L/2 R_v X_v \ln(R_s/R_c)]^{-1} \tag{7}$$

where R_g = grain radius = 3.5×10^{-5} cm for the V produced in this study,

R_s = half the average spacing between point defect sinks = $3. \times 10^{-6}$ cm,

R_c = core radius of a dislocation = 10^{-7} cm,

R_v = void radius = 1.15×10^{-6} cm at 873K,[34]

X_v = void density = 3.2×10^{14} cm^{-3} at 873K,[34] and

L = dislocation density = 10^8 cm^{-2}.

Solving the above equations, the sink efficiencies for vanadium at 873K with a grain size of 0.7 μm are:

$$f_{gb} = 92.3\% \quad (8)$$

$$f_{dis} = 0.3\% \quad (9)$$

$$f_{void} = 7.4\% \quad (10)$$

The void density experimentally obtained by Wiffen[34] was adjusted to account for the presence of a void depletion zone adjacent to the grain boundary.[35]

For the same material with a high dislocation density of 10^{10} cm^{-2}, at 873K the efficiencies become:

$$f_{gb} = 70.8\% \quad (11)$$

$$f_{dis} = 23.2\% \quad (12)$$

$$f_{void} = 6.0\% \quad (13)$$

From this calculation we see that the grain boundary area traps the bulk of the excess vacancies, reducing swelling by 70 - 92%. This effect has been experimentally demonstrated by Singh[36] with a fine-grained austenitic stainless steel. If one can produce deposits of refractory metals with this very small grain size, then the problem of void formation and growth in reactor structural materials would be greatly alleviated.

CONCLUSIONS

Three refractory metals were deposited. The mechanical properties of Mo and Nb were comparable to those of conventionally prepared material. The yield strength of V deposits was superior to wrought V because of its ultrafine (0.7 μm) grain size. Calculations showed that this material should strongly resist void formation and growth when irradiated by fast neutrons at 873K due to vacancy capture by the grain boundaries. In the future, it should be possible to produce refractory metals and their alloys for use in reactor technology with the required property of reduced swelling using HRPVD techniques.

ACKNOWLEDGEMENTS

The authors are grateful to Mr. Terry Webster of Teledyne Wah Chang Albany for the chemical analyses, and the support of CMB-8, Los Alamos Scientific Laboratory, and the Advanced Projects Research Agency (ARPA grant DAHC 15-70-G-15).

REFERENCES

1. R. A. Krakowski et. al., Los Alamos Scientific Laboratory Report LA-5336, March 1974.
2. ASTM Annual Book of Standards, Part 31, 848-851, (1973).
3. B. E. Warren, X-Ray Diffraction, 260-262, (1969).
4. J. B. Nelson and D. P. Riley, Proc. Phys. Soc. (London), 57(3), 160-177, (1945).
5. H. R. Smith Jr., Vacuum Metallurgy, R. F. Bunshah ed., 221-235, (1958).
6. L. Brewer and G. M. Rosenblatt, Trans. AIME, 224, 1268-1271, (1962).
7. B. A. Movchan and A. V. Demchishin, Fiz. Metal. Metallov., 28(4), 83-90, (1969).
8. R. F. Bunshah, J. Vac. Sci. Technol., 11, (1974). To be published.
9. E. O. Hall, Proc. Phys. Soc. (London), B64, 747-753, (1951).
10. N. J. Petch, J. Iron and Steel Inst., 174, 25-28, (1953).
11. T. L. Briggs and J. D. Campbell, Acta Met., 20, 711-724, (1972).
12. R. N. Orava, Trans. AIME, 230, 1614-1622, (1964).
13. R. N. Orava, Refractory Metals and Alloys IV, 117-140, (1967).
14. A. A. Johnson, Phil. Mag., 4(194), 194-199, (1959).
15. A. G. Ingram et. al., Trans. AIME, 230, 1345-1352, (1964).
16. A. T. Churchman, J. Inst. Metals, 88, 221-222, (1960).
17. E. S. Tankins and R. Maddin, Columbium Metallurgy, 343-363, (1960).

18. M. A. Adams et. al., Acta Met., 8, 328-337, (1960).

19. T. C. Lindley and R. E. Smallman, Acta Met., 11, 626-628, (1963).

20. H. Conrad et. al., Mat. Sci. Engr., 2, 157-168, (1967).

21. Z. C. Szkopiak, Mat. Sci. Engr., 9(1), 7-13, (1972).

22. Z. C. Szkopiak, J. Less-Common Metals, 26, 19-24, (1972).

23. D. H. Sherman et. al., Trans. AIME, 242, 1775-1784, (1968).

24. G. Elssner and G. Horz, J. Less-Common Metals, 27, 237-240, (1971).

25. R. H. Van Fossen Jr. et. al., J. Less-Common Metals, 9, 437-451, (1965).

26. T. C. Lindley and R. E. Smallman, Acta Met., 11, 361-371, (1962).

27. Y. S. Belomytsev et. al., Fiz. Metal. Metallov., 27(1), 77-80, (1969(.

28. H. W. Paxton and J. M. Sheehan, in G. L. Miller, Tantalum and Niobium, 406, (1957).

29. R. Q. Barr et. al., Refractory Metals and Alloys III, 17-26, (1966).

30. R. F. Maringer and A. D. Schwope, Trans. AIME, 200, 365-366, (1954).

31. S. C. Srivastava and L. L. Siegle, Met. Trans., 5, 49-52, (1972).

32. W. B. Pearson, Lattice Spacings and Structures of Metals and Alloys, I, 752, (1958).

33. S. D. Harkness et. al., Nucl. Sci. Technol., 9, 24-30, (1970).

34. F. W. Wiffen, Radiation-Induced Voids in Metals, 386-396, (1971).

35. L. E. Thomas and R. M. Fisher, Conf. on Phys. Metall. of Reactor Fuel Elements, to be published.

36. B. N. Singh, Phil. Mag., 29(1), 25-42, (1974).

Caption Legend

Figure 1. Reference Theta Pinch Reactor. Cross section of torus (right); radial blanket segment (left).

Figure 2. Schematic of deposition setup.

Figure 3. Structural zones in condensates (after Movchan and Demchishin[7]).

Figure 4. Surface of molybdenum deposited at 873K. Zone 1 morphology. 1570X.

Figure 5. Surface of molybdenum deposited at 1073K showing elongated grain morphology. 408X.

Figure 6. Cross section of molybdenum deposited at 1073K showing epitaxial growth of grains. 540X.

Figure 7. Cross section of niobium showing equiaxed grains. 500X.

Figure 8. Transmission electron micrograph of deposited vanadium. 34000X.

Figure 9. Yield strength versus inverse square root of grain diameter for molybdenum.

Figure 10. Fracture strength versus inverse square root of grain diameter for molybdenum.

Figure 11. Yield strength versus inverse square root of grain diameter for niobium.

Figure 12. Yield strength versus inverse square root of grain diameter for vanadium.

Figure 13. Lattice parameter of molybdenum condensates versus substrate temperature.

TABLE I

Niobium First Wall Parameters for the Controlled Thermonuclear Reactor

Definition	Value
Fluence of 14.4 MeV neutrons	$2.84 \times 10^{21}/cm^2$-yr.
Helium production	270 at. ppm/yr.
Hydrogen production	890 at. ppm/yr.
Transmutation rate	1.4 at. %/yr.
Atom displacement rate	120 dpa/yr.
Operating temperature	773 - 1273K
Niobium thickness	0.100 cm
Alumina insulator thickness	0.030 cm
Inside radius of niobium wall	50.00 cm
Energy deposition	$494\ J/cm^3$
Maximum tangential stress	$15\ kg/mm^2$

TABLE II

Chemical Analysis of Molybdenum Evaporants and Deposits
(ppm by weight)

	Thermo Electron[1] evaporant stock	Deposit Mo-A-5 (fr. T. E. stock)	Climax Moly. evaporant stock	Deposit Mo-E-3-3 (fr. Climax stock)
C	50	70	40	30
O	9	750	50	150
N	2	25	5	8
H	1	23	5	8
Cu	—	10	10	60
Fe	30	95	37	45
Ni	—	10	10	10
Si	20	147	120	40
Ti	—	13	10	10

[1] Supplier's analysis

TABLE III

Chemical Analysis of Niobium Evaporant and Deposits (ppm by weight)

	Teledyne Wah Chang evaporant stock	Deposit Nb-A-2-2	Deposit Nb-A-2-3
C	35	80	70
O	<50	350	360
H	2.4	15	8
N	33	33	32
Al	<20	<20	<20
B	<1	<1	<1
Ca	<20	<20	<20
Cd	<5	<5	<5
Co	<10	<10	<10
Cr	<20	50	<20
Cu	<40	<40	<40
Fe	<50	<50	58
Hf	<50	<50	<50
Mg	<20	<20	<20
Mn	<20	<20	<20
Mo	<20	25	50
Ni	<20	<20	<20
Pb	<20	<20	<20
Si	52	80	58
Sn	<10	<10	10
Ta	110	612	826
Ti	<40	<40	56
V	<20	<20	<20
W	43	—	—
Zr	<100	<100	324

TABLE IV

Chemical Analysis of Vanadium Evaporant and Deposits (ppm by weight)

	Teledyne Wah Chang evaporant stock	Deposit V-A-3-2	Deposit V-A-3-3
C	125	120	140
O	110	470	540
N	110	84	99
H	<5	19	9
Al	88	72	70
B	<1	<1	<1
Cu	<40	<40	<40
Fe	89	53	<50
Mg	34	<20	<20
Mn	<20	<20	<20
Mo	<20	120	115
Nb	<1000	<1000	<1000
Si	539	135	140
Ta	<1000	<1000	<1000
Ti	<50	<50	<50
W	<500	<100	<100

TABLE V

Morphology Zone Boundary Temperatures[1]

Material	Zone 1	Zone 2	Zone 3
Metals	$<0.3\ T_m$ [(2)]	$0.3 - 0.45\ T_m$	$>0.45\ T_m$
Oxides	$0.26\ T_m$	$0.25 - 0.45\ T_m$	$0.45\ T_m$

[1] From Movchan and Demchishin[7]

[2] T_m is the absolute melting temperature

Calculated Transition Temperatures

Material	T_m	T_1	T_2
Molybdenum	2610°C 2883 K	592°C 865 K	1024°C 1297 K
Niobium	2468°C 2741 K	549°C 822 K	960°C 1233 K
Vanadium	1890°C 2163 K	376°C 649 K	700°C 973 K

TABLE VI

Mechanical Properties of Molybdenum Deposits

Sample*	Deposition Temp (K)	Grain Size (μm)	Crosshead Speed (cm/min)	Yield Strength (kg/mm²)	Yield Strength (ksi)	UTS (kg/mm²)	UTS (ksi)	% R. A.	Diamond Pyramid Hardness (kg/mm²) Surface	Diamond Pyramid Hardness (kg/mm²) Edge	Bend Ductility %
B-1	1263	530	0.05	14.4	20.5	18.6	26.5	5.3	191.0±6.5	----	0.6
B-2	977	83	0.05	24.2	34.4	28.1	40.0	0.8	169.7±29.5	216.5±11.8	----
B-3	1077	19	0.05	38.0	54.0	43.6	62.0	1.0	186.0±12.2	184.0±9.2	<0.8
B-4	1083	17.5	0.005	21.8	31.0	29.9	42.5	11.4	----------	----	----
B-5	1089	15.5	0.005	25.3	36.0	29.2	41.5	1.9	----------	----	<0.6
B-7	1083	15.6	0.005	25.3	36.0	29.7	42.3	4.8	----------	----	0.5
B-8	1089	15.5	0.005	25.3	36.0	----	----	----	----------	----	----
B-10-2	1075	51	0.005	15.3	21.8	30.1	42.8	2.5	----------	----	5.4
B-11-1	972	13	0.005	31.5	44.8	----	----	----	----------	----	0.9
B-11-2	972	13	0.005	27.4	39.0	41.1	58.5	8.5	----------	----	0.9
C-1-2	873	56	0.005	10.6	15.1	15.0	21.3	4.3	----------	----	<0.6

Hall Petch Parameters

	σ_0 (kg/mm²)	k (kg/mm$^{3/2}$)
Yield at 0.05cm/min	9.6	4.9
Yield at 0.005cm/min	-2.7	3.54
Fracture at 0.05cm/min	13.1	4.22
Fracture at 0.005cm/min	8.9	3.0

* Samples B-1 through B-5 synthesized from Thermo Electron evaporant stock, balance from Climax Molybdenum evaporant stock.

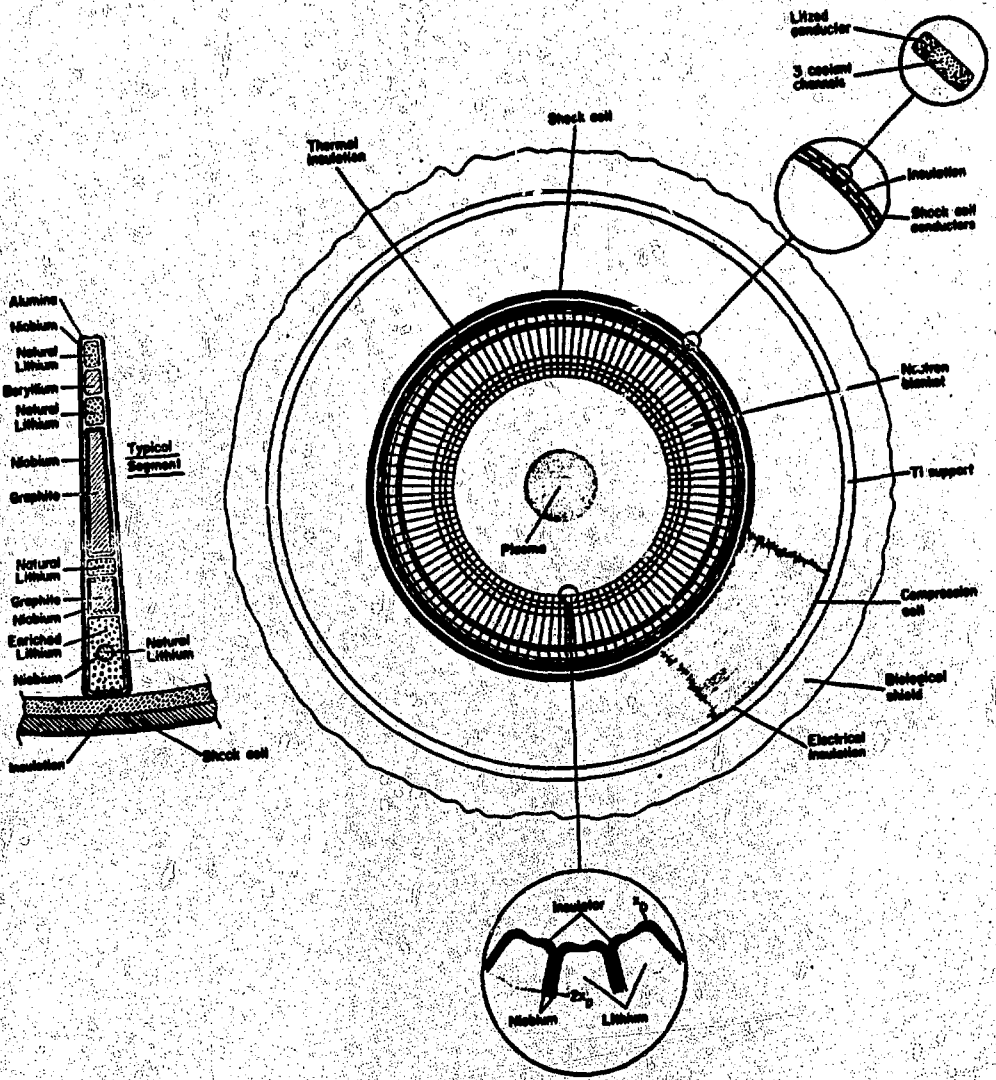
Litzed conductor
3 coolant channels
Insulation
Shock coil conductors
Thermal insulation
Shock coil
Neutron blanket
Ti support
Plasma
Compression coil
Biological shield
Electrical insulation
Alumina
Niobium
Natural Lithium
Beryllium
Natural Lithium
Niobium
Graphite
Typical Segment
Natural Lithium
Graphite
Niobium
Enriched Lithium
Natural Lithium
Niobium
Insulation
Shock coil
Insulator
Niobium
Lithium

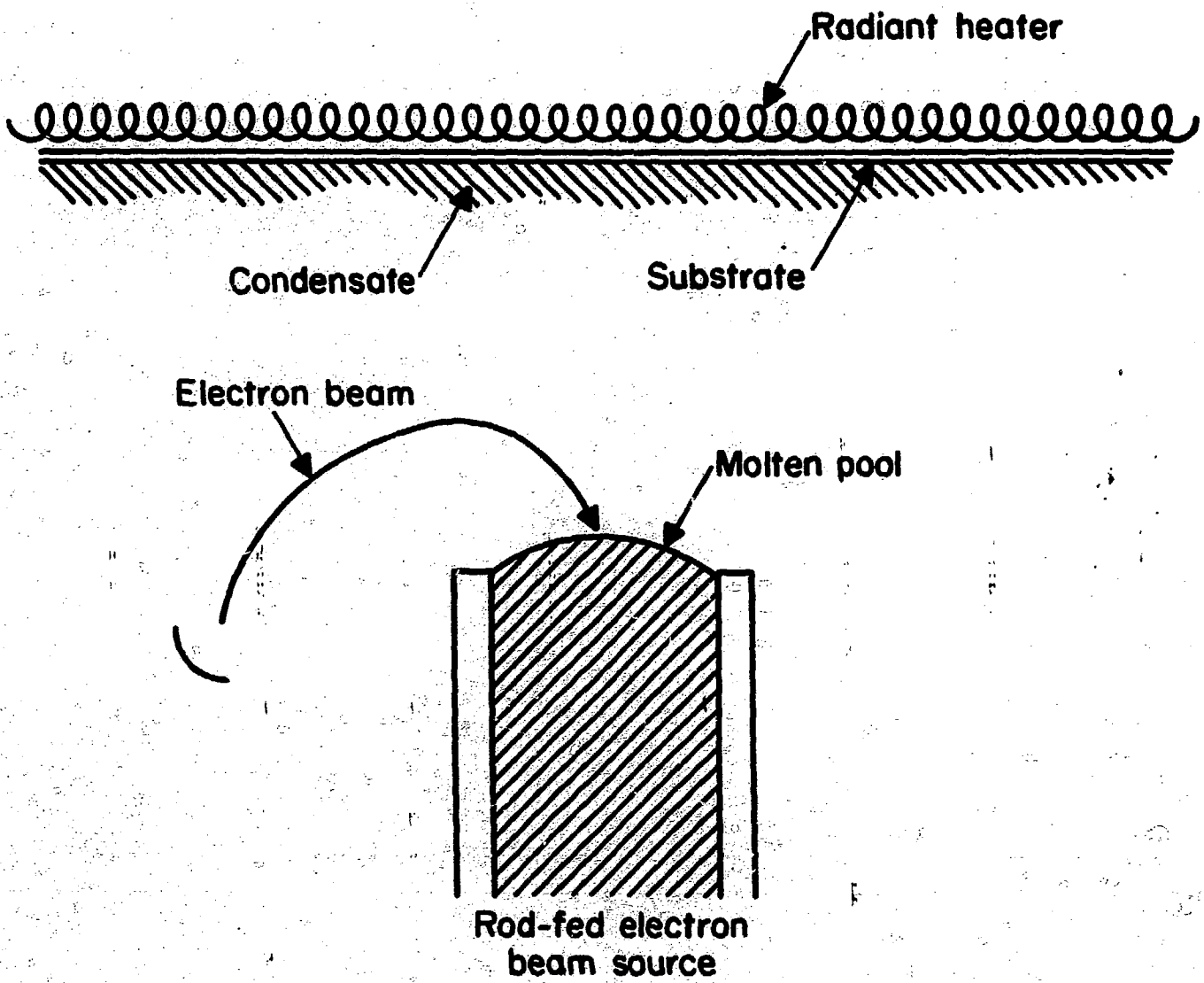
Radiant heater
Condensate
Substrate
Electron beam
Molten pool
Rod-fed electron
beam source

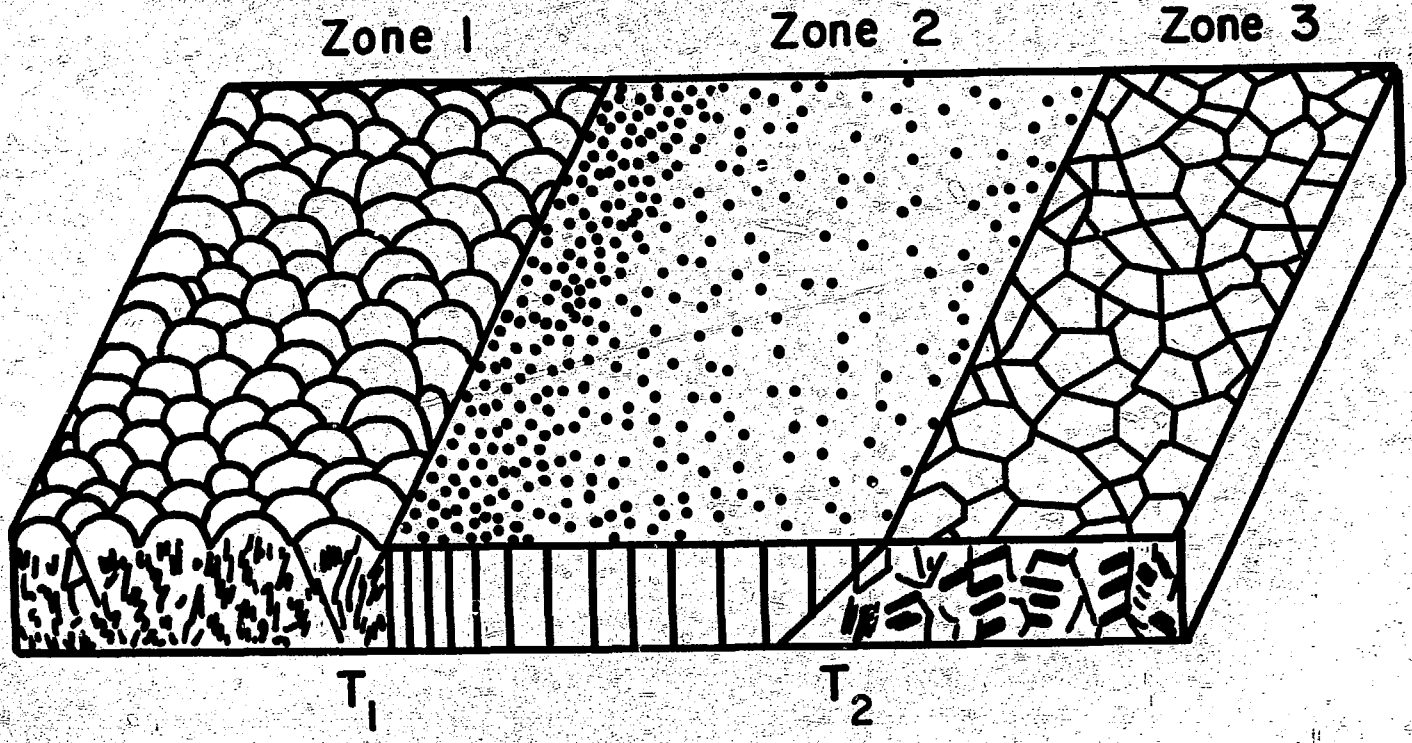
Zone 1
Zone 2
Zone 3
T_1
T_2
Temperature

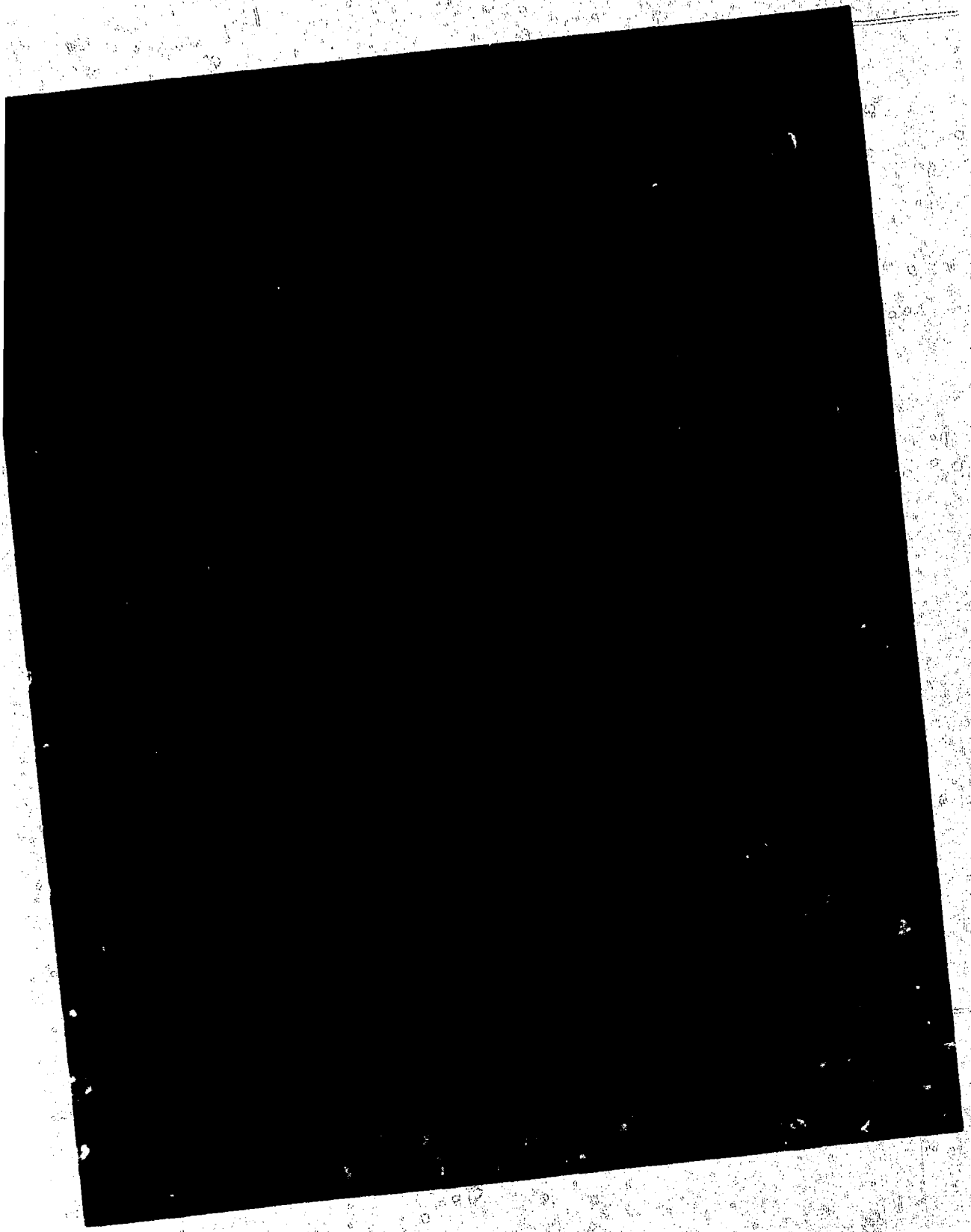

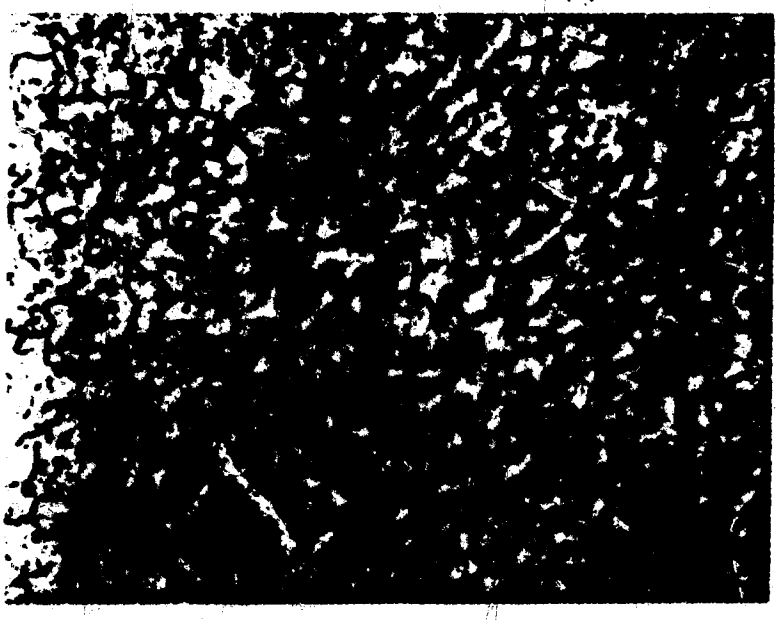

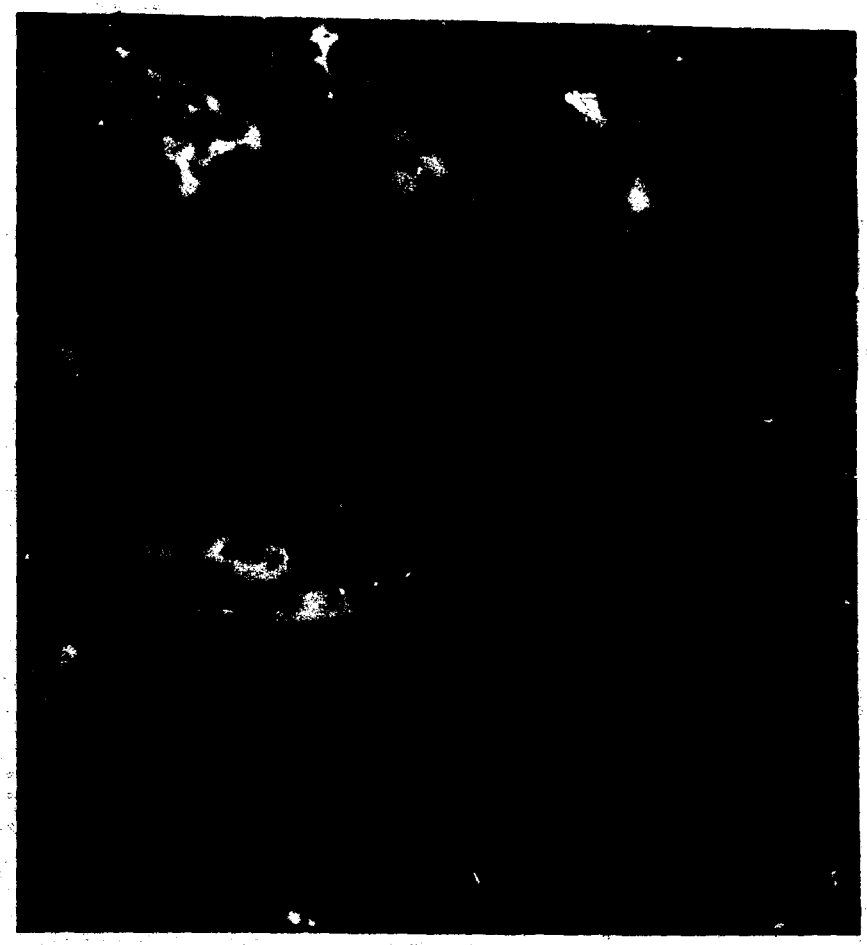

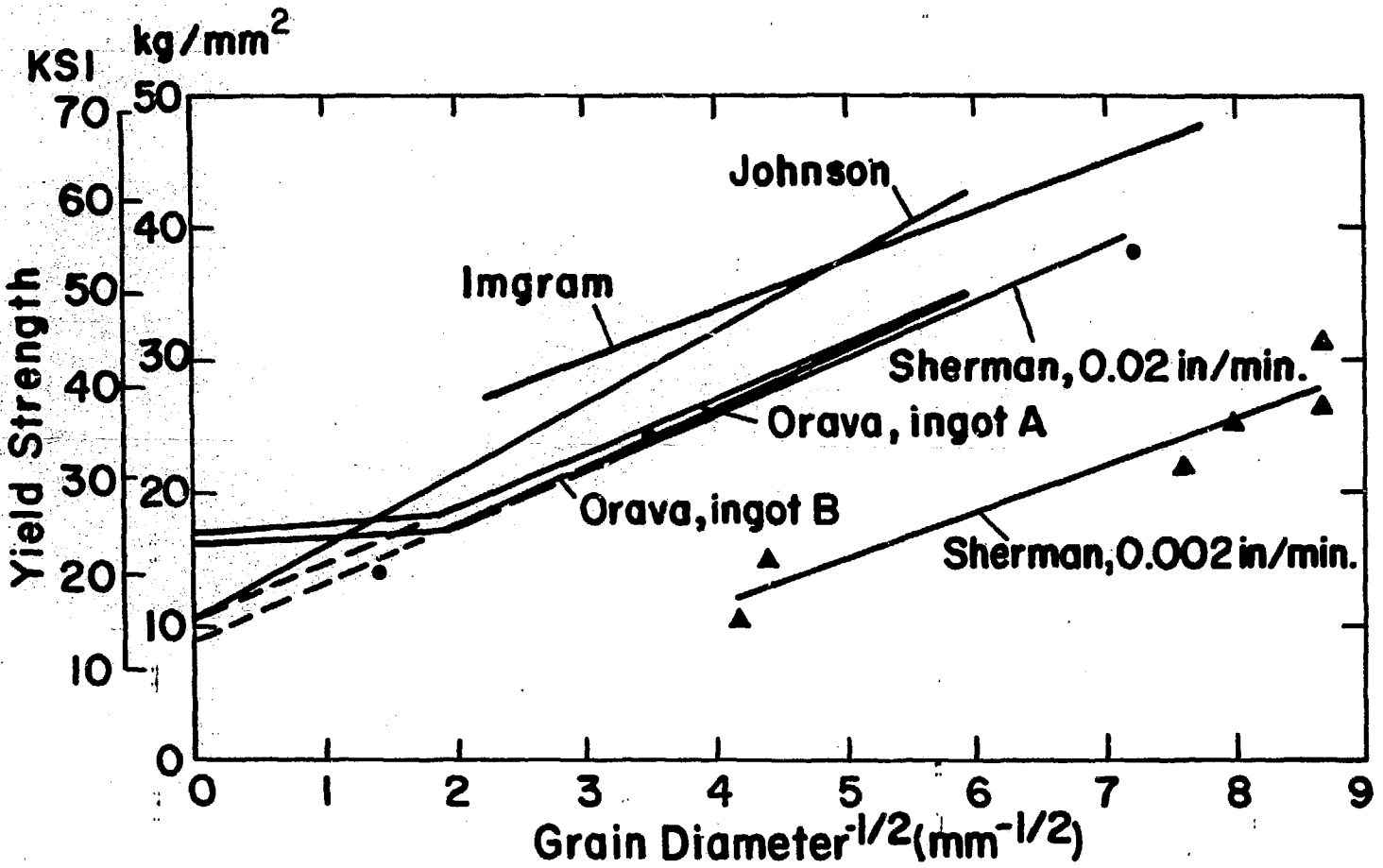
KSI
kg/mm²
70
60
50
40
30
20
10
50
40
30
20
10
0
Yield Strength
Johnson
Imgram
Sherman, 0.02 in/min.
Orava, ingot A
Orava, ingot B
Sherman, 0.002 in/min.
0
1
2
3
4
5
6
7
8
9
Grain Diameter$^{-1/2}$(mm$^{-1/2}$)

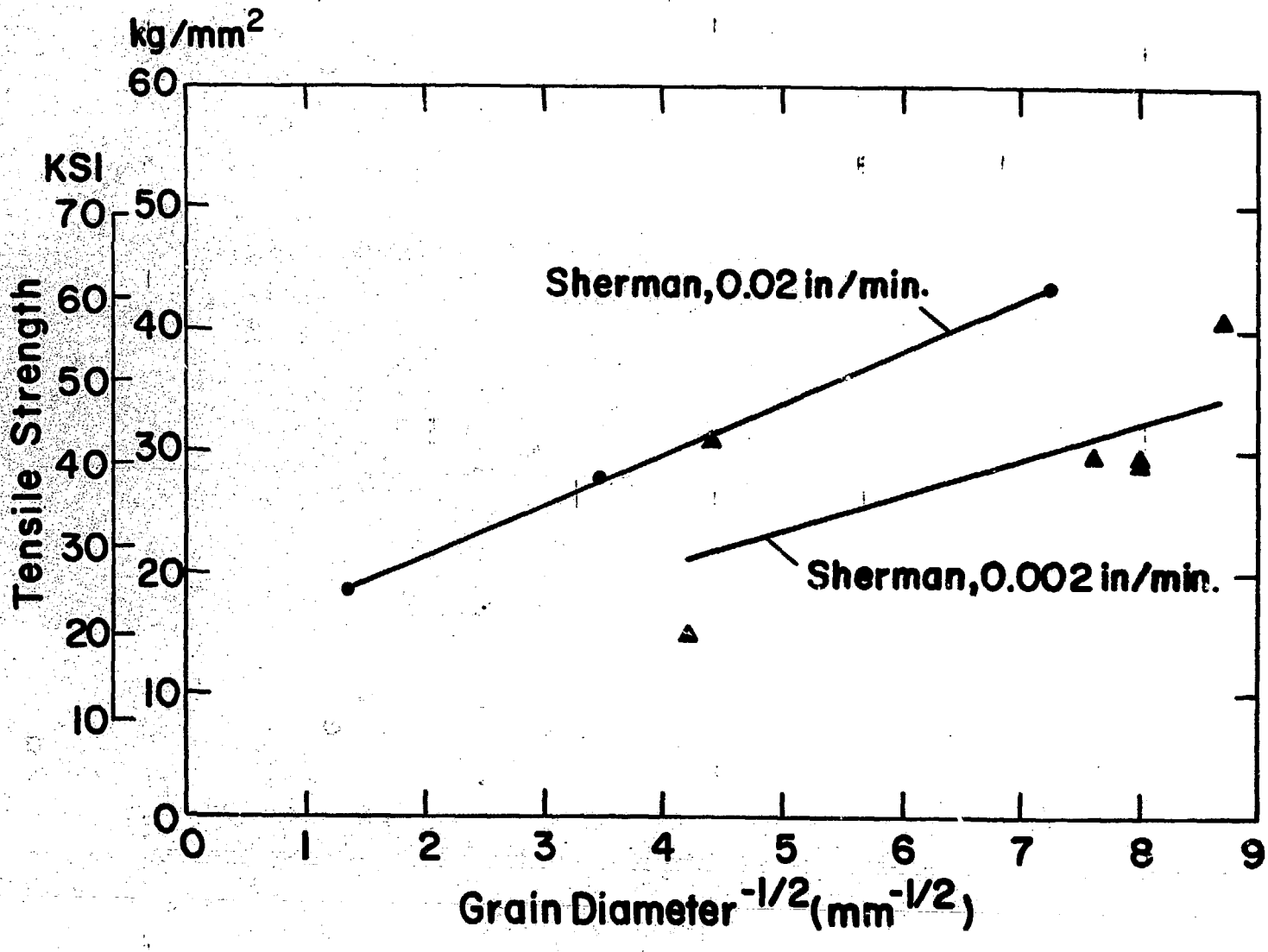
kg/mm2
60
KSI
70
50
Tensile Strength
60
40
50
30
40
30
20
20
10
10
0
0
1
2
3
4
5
6
7
8
9
Sherman, 0.02 in/min.
Sherman, 0.002 in/min.
Grain Diameter -1/2 (mm -1/2)

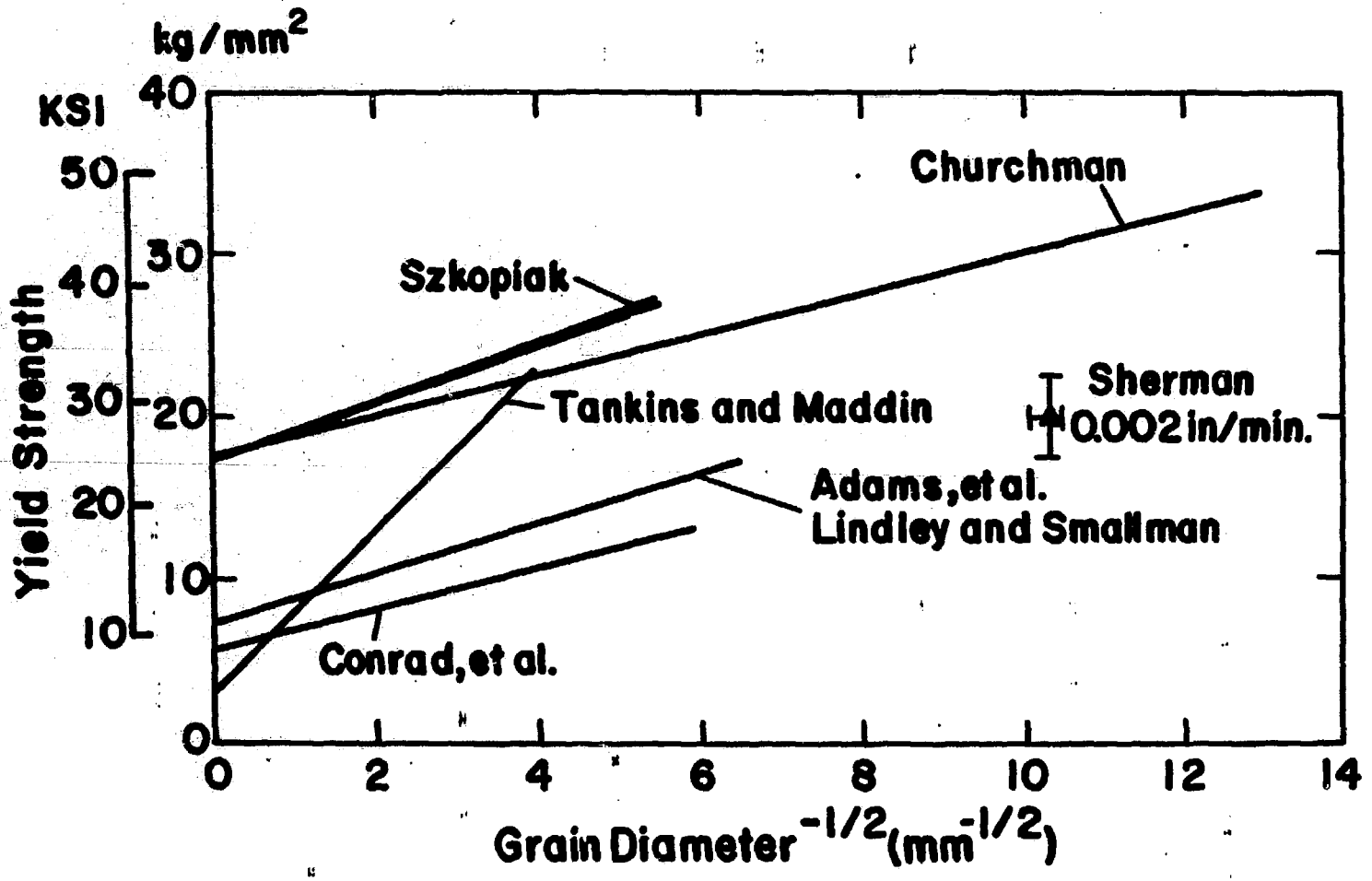
kg/mm²
KSI
40
50
30
40
20
30
10
20
0
10
Yield Strength
Churchman
Szkopiak
Tankins and Maddin
Sherman
0.002 in/min.
Adams, et al.
Lindley and Smallman
Conrad, et al.
0
2
4
6
8
10
12
14
Grain Diameter $^{-1/2}$ (mm$^{-1/2}$)

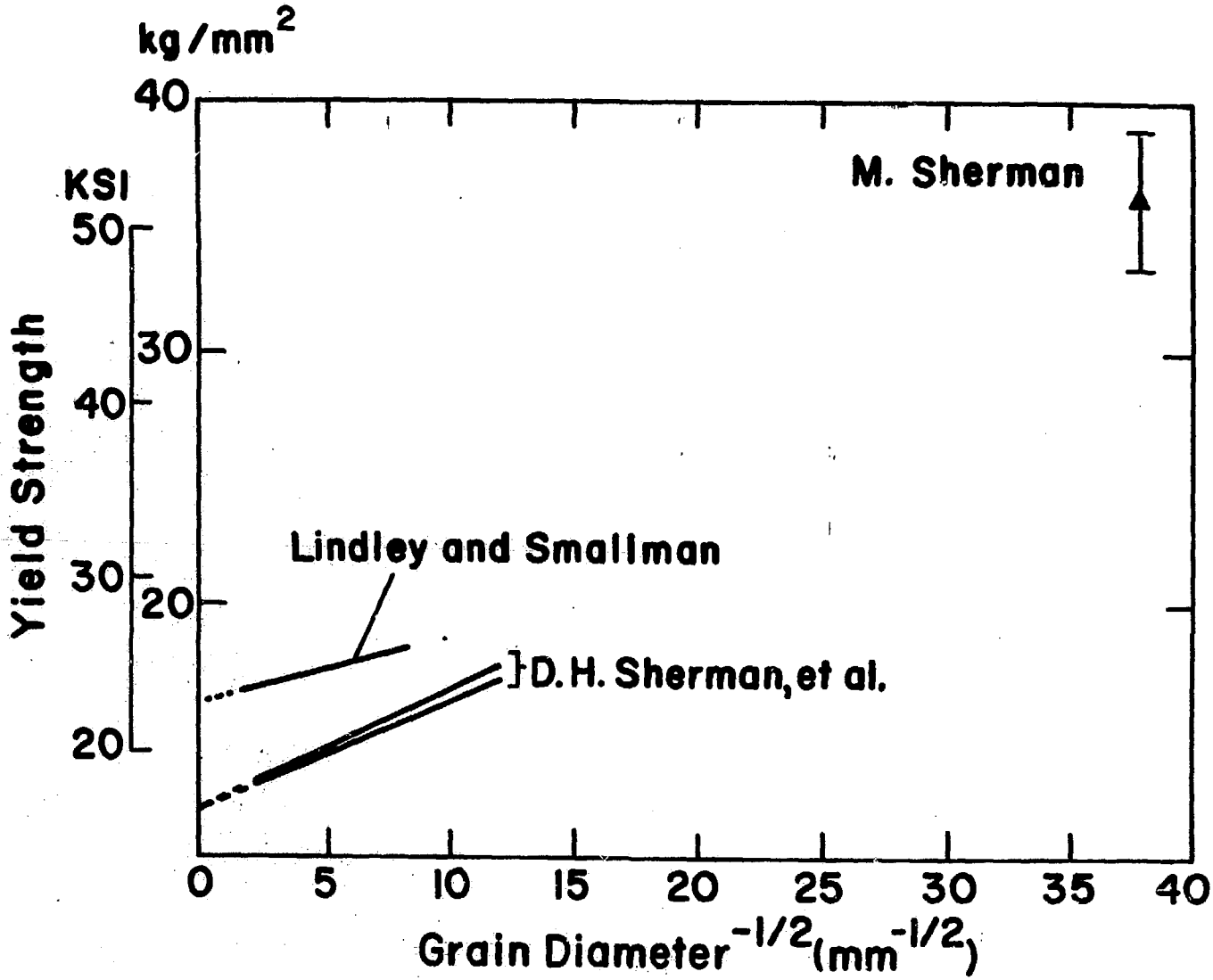
kg/mm²
40
KSI
50
30
40
30
20
20
Yield Strength
M. Sherman
Lindley and Smallman
D. H. Sherman, et al.
0
5
10
15
20
25
30
35
40
Grain Diameter $^{-1/2}$ (mm$^{-1/2}$)

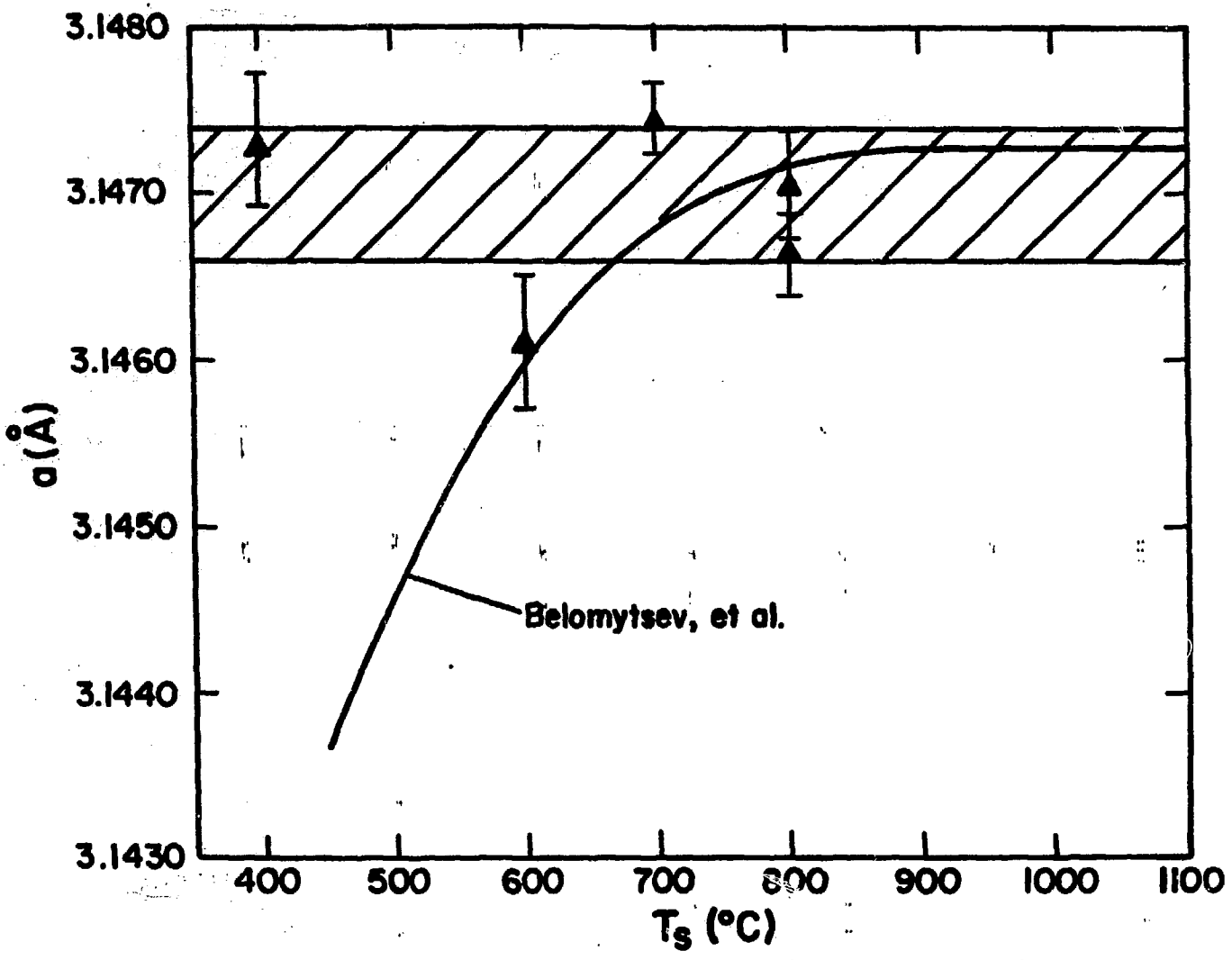

Lattice Parameter of Molybdenum Condensates vs Substrate Temperature